analytical chemistry

pubs.acs.org/ac

Article

Quantitation of Trastuzumab and an Antibody to SARS-CoV-2 in Minutes Using Affinity Membranes in 96-Well Plates

Hui Yin Tan, Junyan Yang, Jacqueline C. Linnes, Christopher J. Welch, and Merlin L. Bruening*

Cite This: *Anal. Chem.* 2022, 94, 884−891

Read Online

ACCESS | Metrics & More | Article Recommendations | Supporting Information

ABSTRACT: Quantitation of therapeutic monoclonal antibodies (mAbs) in human serum could ensure that patients have adequate levels of mAbs for effective treatment. This research describes the use of affinity, glass-fiber membranes in a 96-well-plate format for rapid (<5 min) quantitation of the therapeutic mAb trastuzumab and a mAb against the SARS-CoV-2 spike protein. Adsorption of a poly(acrylic acid)-containing film in membrane pores and activation of the −COOH groups in the film enable covalent-linking of affinity peptides or proteins to the membrane. Passage of mAb-containing serum through the affinity membrane results in mAb capture within 1 min. Subsequent rinsing, binding of a secondary antibody conjugated to a fluorophore, and a second rinse yield mAb-concentration-dependent fluorescence intensities in the wells. Calibration curves established from analyses on different days have low variability and allow determination of mAb levels in separately prepared samples with an average error <10%, although errors in single-replicate measurements may reach 40%. The assays can occur in diluted serum with physiologically relevant mAb concentrations, as well as in undiluted serum. Thus, the combination of 96-well plates containing affinity membranes, a microplate reader, and a simple vacuum manifold affords convenient mAb quantitation in <5 min.

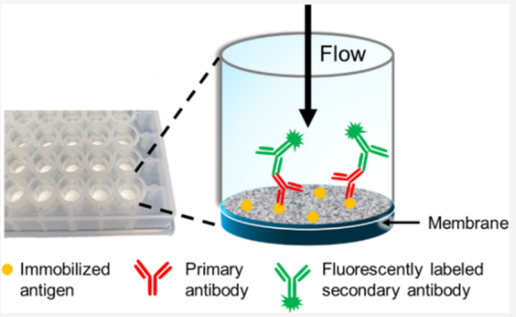

INTRODUCTION

This paper demonstrates selective and fast (<1 min) capture of monoclonal antibodies (mAbs) using 96-well plates containing glass-fiber membranes modified with a mimotope (a peptide that mimics an antibody epitope) or a SARS-CoV-2 antigen. Subsequent binding of fluorescently labeled secondary antibodies allows quantification of captured mAbs in minutes, even from undiluted serum. Thus, this research offers a simple, rapid method for immunoassays, which are fundamental analytical tools for clinical diagnostics,[1,2] food testing,[3,4] therapeutic drug monitoring,[5,6] and clinical pharmacokinetics studies for drug discovery.[7,8] The global market for immunoassays was $18 billion in 2018 and should grow due to increases in chronic and infectious diseases worldwide.[9]

Immunoassays are ubiquitous, but they often require hours to complete.[10−12] Enzyme-linked immunosorbent assays (ELISAs) are extremely successful and offer very low detection limits. For example, commercial kits have detection limits as low as 16 pg/mL for human TNF alpha[10] and 8 pg/mL for human VEGF.[11] However, these kits typically require at least 2 h for analyses. Bead-based ELISAs and automated instrumentation enable such analyses in about 1 h,[13−15] although the techniques are labor-intensive or require specialized instrumentation. He et al. recently developed miniaturized 96-well plates that require only 5 μL of the sample for each well and minimal equipment (a pipette and a magnet).[16] ELISA using streptavidin beads in femtoliter-sized wells improves the limit of protein detection to sub-attomolar concentrations, but analysis times are still 2 h.[17]

Determination of the concentration of therapeutic mAbs is important for the development and manufacturing of immunotherapeutic drugs[18,19] and for monitoring the levels of these mAbs in patients.[20−22] One challenge in mAb therapies is high patient-to-patient variability; the levels of mAbs in patients may differ four- to ten-fold between individuals at the same time after drug administration.[20,23,24] Low mAb concentrations lead to ineffective treatments, whereas high levels may cause side effects in some cases.[20,22,25,26] Hence, a rapid, inexpensive immunoassay could potentially enable better control of mAb dosing for maximized efficacy.

This paper describes assays developed for two model mAbs: trastuzumab and a mAb against SARS-CoV-2. Trastuzumab is a mAb that targets human epidermal growth factor receptor 2 (HER2) in tumors such as breast cancer, metastatic gastric cancer, and gastroesophageal junction adenocarcinoma.[27−29] In clinical settings, trastuzumab has a trough concentration

Received: August 24, 2021
Accepted: December 20, 2021
Published: January 4, 2022

https://doi.org/10.1021/acs.analchem.1c03654
Anal. Chem. 2022, 94, 884−891

range of 20−440 μg/mL in patient plasma[30] with a desired value of >20 μg/mL.[31,32] The variations in concentrations among patients depend on the number of metastatic sites, the concentration of HER2, and body weight.[33,34] Yang et al. showed that a higher trastuzumab trough concentration correlates with longer patient survival.[35]

Like drugs for metastatic cancers, mAbs against coronavirus disease 2019 (COVID-19) could improve patient survival in this deadly pandemic. Despite the massive scale of the COVID-19 pandemic, the U. S. Food and Drug Administration (FDA) approved only a few therapeutic drugs under Emergency Use Authorization (EUA). These drugs include remdesivir (an antiviral drug),[36−38] bamlanivimab/etesevimab (anti-SARS-CoV-2 mAbs),[39] and convalescent plasma,[40,41] which refers to transfusion of plasma collected from individuals who recovered from COVID-19 into recently infected COVID-19 patients. A rapid assay for SARS-CoV-2 antibodies would aid in selecting serum donors with high levels of antibodies for efficient treatment. Additionally, quantitative tests for antibodies against SARS-CoV-2 may be helpful in evaluating the immunity developed from a previous infection or vaccination to estimate the protection of an individual or community from the virus. Finally, assays for therapeutic mAbs used in COVID-19 treatment could prove useful in personalized dosing strategies.

Our group developed nylon membranes modified with peptide mimotopes for capture and analysis of mAbs using spin columns.[42,43] In general, membrane adsorbers are attractive for rapid capture of various molecules due to convection and short radial diffusion distances in micron-sized pores.[43−47] Adsorption of a poly(acrylic acid) (PAA)-containing film in membrane pores followed by activation of the film enables immobilization of affinity groups at high densities.[42,43,48−50] Modification of pores with either polymer brushes[45−47] or layer-by-layer films[42,43,51] can create affinity membranes with high binding capacities, and membrane modification using layer-by-layer deposition of a few polyelectrolyte layers is very convenient.

Flow through μm-sized pores combined with a high surface area-to-volume ratio in mimotope-modified membranes allows capture of antibodies within minutes. Moreover, the high mimotope density gives extensive mAb capture even with μM dissociation constants for mimotope−antibody complexes. Analysis of eluted mAbs using native tryptophan fluorescence occurred in 20 min using spin membranes.[42] Separately, our group reported the fabrication of nickel-containing membranes for rapid polyhistidine-tagged protein purification.[48,51] The nickel-functionalized membranes allow convenient immobilization of polyhistidine-tagged proteins in an oriented fashion, which might be crucial for affinity binding of mAbs.

The present work advances membrane-based mAb analysis through the use of a fluorescent secondary antibody and glass-fiber membranes in 96-well plates. Using a vacuum manifold, flow of antibody-containing serum, rinsing solutions, and a secondary-antibody solution through a membrane can occur in around 3 min. Subsequent fluorescence detection on a plate reader completes the analysis in minutes. Such rapid and quantitative assays may prove useful for monitoring antibody levels during treatment, manufacturing, and research.

EXPERIMENTAL SECTION

Materials. Glass-fiber membranes (Pall Corporation, A/C Glass Fiber 1 μm pores, 25 mm diameter, 254 μm thick) were cleaned in a UV/O_3 chamber (Jelight, model 18) for 10 min prior to modification. AcroPrep Advance 96-well plates (350 μL well volume, 1 μm pores) were acquired from Pall Corporation. The plates contain 660 μm-thick glass-fiber membranes at the bottom of 0.8 cm-diameter wells. The Tra19 peptide (KGSGSGSQLGPYELWELSH) was synthesized by GenScript with a purity greater than 95%. Poly(acrylic acid) (PAA, average molecular weight ∼250,000 Da, 35% aqueous solution), polyethylenimine (PEI, branched, M_w = 25,000 Da), *N*-(3-dimethylaminopropyl)-*N*′-ethylcarbodiimide hydrochloride (EDC), *N*-hydroxysuccinimide (NHS), Tween-20 surfactant, sodium phosphate monobasic monohydrate, sodium phosphate dibasic heptahydrate, sodium chloride, *Nα*,*Nα*-bis(carboxymethyl)-L-lysine (aminobutyl NTA), imidazole, and human serum were purchased from Sigma-Aldrich. Deidentified patient serum samples were purchased from BioChemEd Services. Poly(vinyl) alcohol (PVA, 99−100% hydrolyzed, approximate molecular weight 8600 Da) and nickel (II) sulfate hexahydrate were acquired from Acros Organics. Trastuzumab (Genentech) was used from its therapeutic formulation. Anti-SARS-CoV-2 spike receptor-binding domain (RBD) antibody [Chimeric mAb, Human IgG1 (S1N-M130)] was purchased from AcroBiosystem, and SARS-CoV-2 Spike RBD protein (his-tagged at the C-terminus, CHO-expressed) was purchased from GenScript. Goat anti-human IgG H&L (Cy5) preadsorbed was acquired from Abcam. Buffers were prepared using analytical-grade chemicals and deionized water (Milli-Q, 18.2 MΩ cm).

Immobilization of Tra19 in Porous Glass-Fiber Membranes in 96-Well Plates. The procedure for immobilization of a peptide mimotope in glass-fiber membranes includes modifying the membranes with a $(PEI/PAA)_2$ film, activating the −COOH groups of PAA, and allowing these groups to react with the free amine groups of Tra19. To deposit the first layer of PEI, 100 μL of 2 mg/mL branched PEI at pH 3 was added to the desired wells in a 96-well plate containing 1 μm-pore glass-fiber membranes. After 5 min of incubation, the solution was pulled through the membrane using a vacuum manifold. This procedure was repeated twice more with a fresh PEI solution to increase the PEI coverage, and the wells were washed with 1 mL of water with applied vacuum. Next, 100 μL of 1.1 mg/mL PAA in 0.5 M NaCl, pH 3 was added to each well, incubated for 5 min, and pulled through the membrane using vacuum. This PAA adsorption procedure was repeated twice more with a fresh solution to increase the coverage with PAA, and the wells were each washed with 1 mL of water. Additional PEI and PAA layers were deposited similarly.

Activation of the carboxylic acid groups of PAA to *N*-hydroxysuccinimidyl esters employed the addition of 100 μL of 40 mM EDC and 40 mM NHS to each well, incubation for 10 min, and removal of the solution with vacuum. The procedure was repeated five more times with a fresh EDC/NHS solution and each well was then washed with 2 mL of water. Finally, 100 μL of 1.5 mg/mL Tra19 in water at pH 9 (pH adjusted with NaOH) was added to each well, incubated for 10 min, and pulled through the membrane. The Tra19 solution was recovered from the vacuum manifold trough and 100 μL was added back to each well for 10 min of incubation (we observe a loss of 10−20% of the solution after vacuum filtering. The recovered solution volume was compensated with more stock solution to give 100 μL for re-incubation). This incubating and passing of the Tra19 solution through the well were performed

https://doi.org/10.1021/acs.analchem.1c03654
Anal. Chem. 2022, 94, 884−891

a total of six times. Finally, the wells were rinsed with 2 mL of water using vacuum. Cross-linking of the PEI/PAA films due to the reaction of some of the amines of PEI with active esters likely increases film stability.

Immobilization of Tra19 in a 2 cm-Diameter Glass-Fiber Membrane. Using a membrane holder and a peristaltic pump,[42] 5 mL of 2 mg/mL branched PEI at pH 3 was circulated through the membrane for 15 min at 1 mL/min, and the membrane was washed with 10 mL of water. Subsequently, 5 mL of 1.1 mg/mL PAA in 0.5 M NaCl, pH 3, was circulated through a 2 cm-diameter glass-fiber membrane at 1 mL/min for 15 min, followed by a 10 mL water wash. Then, another bilayer of PEI/PAA was deposited as described above. Activation of the membrane for Tra19 immobilization involved circulating 5 mL of 40 mM EDC and 40 mM NHS for 1 h at 1 mL/min. After a 10 mL water rinse, 1 mL of 1 mg/mL Tra19 in pH 9 water (pH adjusted with NaOH) was circulated through the membrane for 1 h at 1 mL/min. A final 10 mL water rinse was employed to remove unbound Tra19. The load, permeate, and washing solutions during Tra19 immobilization were collected, and the intrinsic tryptophan fluorescence of the peptide was measured using a Synergy H1 microplate reader by exciting at 280 nm and measuring emission from 300 to 400 nm, with peak emission at 348 ± 2 nm. A calibration curve was established using standards of Tra19 at pH 9 to determine the Tra19 concentration in the load, permeate, and washes. We diluted the permeate aliquots 20-fold with water prior to fluorescence measurements, so absorbance due to liberated NHS would not interfere with the analyses.

To mimic the modification of membranes in 96-well plates, we also modified the 2 cm membranes using incubation, passage of the solution through the membrane at 5 mL/min using a peristaltic pump, and recycling of the Tra19 solutions for subsequent repeat incubations. This procedure employed the same incubation times and five times the solution volumes used for the modifications of the 96-well plates. The increased volume approximately correlates with the higher surface area of the 2 cm membranes.

Breakthrough Curves in Tra19-Modified Membranes. Using a peristaltic pump, a 2 cm-diameter Tra19-modified membrane was rinsed with 5 mL of 20 mM phosphate buffer, pH 7.4, in 500 mM NaCl at 1 mL/min prior to a passage of 5 mL of 100 μg/mL trastuzumab (in the same buffer solution) through the membrane at a flow rate of 0.5 or 5 mL/min. Multiple fractions of the permeate were collected in preweighed tubes and the permeate volume of each fraction was calculated based on mass. The concentrations of trastuzumab in the permeate fractions were determined using native fluorescence measured using a Synergy H1 microplate reader (excitation at 280 nm, emission at 330 nm ± 2 nm) with a calibration curve based on trastuzumab standards in buffer.

Binding of Trastuzumab from Diluted Serum in 96-Well Plates Containing Tra19-Modified Membranes. With vacuum running, each well was rinsed with 2 mL of wash buffer A (20 mM pH 7.4 phosphate buffer, 0.5 M NaCl, and 0.1% Tween-20), and then, 0.5 mL of solution containing varied concentrations of trastuzumab (0−4 μg/mL) in 1% (v/v) human serum in 20 mM phosphate buffer (pH 7.4, 0.5 M NaCl) was loaded in each well. Subsequently, during vacuum filtration, the plate was washed with 2 mL of wash buffer A in each well. One milliliter of 10 μg/mL secondary antibody (polyclonal anti-human IgG conjugated to Cy-5) in 20 mM phosphate buffer, pH 7.4, and 0.5 M NaCl was then vacuum-filtered through each well, followed by 2 mL of wash buffer A. The concentration of mAb was determined by measuring the fluorescence of Cy5 bound to the well (excitation at 645 nm, emission at 670 nm) using a Synergy H1 microplate reader and comparing the fluorescence intensity to a calibration curve obtained using known concentrations of primary antibodies in similar binding experiments.

Experiments followed the same protocol for pooled serum and individual patient sera. Because the pooled serum purchased from Sigma-Aldrich was heat-inactivated and filtered, the serum from individual patients was also heat-treated and filtered following established methods (Gemini Bio).[52]

Immobilization of RBD-his Protein in Porous Glass-Fiber Membranes in 96-Well Plates. To capture an antispike antibody, we immobilized a polyhistidine-tagged form of the COVID-19 spike RBD protein (RBD-his) in membranes. The method for adsorption of polyelectrolyte layers in the membrane was the same as described above. After activation with EDC/NHS solution using the above-mentioned procedure, 100 μL of 0.1 M aminobutyl NTA in a pH 10.5 solution (pH adjusted with NaOH) was added to the well and incubated for 10 min before removing the solution with vacuum. This step was repeated five more times using recycled solution. Then, 100 μL of 0.1 M nickel sulfate was added, incubated for 10 min, and removed by vacuum, and this process was repeated five more times using recycled solution. To immobilize the RBD-his, 100 μL of 0.1 mg/mL RBD-his in 20 mM phosphate buffer, pH 7.4, and 150 mM NaCl was incubated in each well for 10 min and vacuum-filtered to recover the RBD-his solution, and the solution was reapplied to each well for five more incubation and filtration steps. Finally, each well was washed with 2 mL of a pH 7.4 solution containing 20 mM phosphate buffer and 150 mM NaCl. Due to the high cost of the recombinant RBD-his, we did not quantify its immobilization.

Binding of Antispike mAb in Diluted Serum to an RBD-his-Functionalized 96-Well Plate. With applied vacuum, the 96-well plate was rinsed with 2 mL of wash buffer A, and 0.5 mL of diluted serum spiked with different concentrations of antispike mAb (0−10 μg/mL antispike in serum diluted with 20 mM pH 7.4 phosphate buffer containing 0.5 M NaCl and 50 mM imidazole) was loaded into each well. This was followed by 1 mL of wash buffer B (20 mM pH 7.4 phosphate buffer in 0.5 M NaCl and 50 mM imidazole), 1 mL of wash buffer A, and 0.5 mL of 20 μg/mL secondary antibody (polyclonal anti-human IgG conjugated to Cy-5) in pH 7.4 phosphate (20 mM) buffer containing 0.5 M NaCl, 1 mL of wash buffer B, and 1 mL of wash buffer A. Finally, the fluorescence of the secondary-antibody-containing well (excitation at 645 nm and emission at 670 nm) was measured using a Synergy H1 microplate reader. A calibration curve was prepared using capture of the antispike mAb at different concentrations, binding of the labeled secondary antibody, and determination of the fluorescence intensity of Cy5 at 670 nm.

RESULTS AND DISCUSSION

The steps in the analytical procedure include modification of the membrane with affinity molecules, capture of a specific mAb, binding of a fluorescently labeled secondary antibody, and measurement of the well fluorescence (Figure 1). Thus,

https://doi.org/10.1021/acs.analchem.1c03654
Anal. Chem. 2022, 94, 884−891

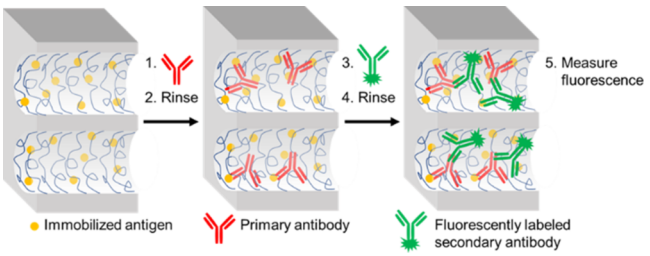

Figure 1. Scheme of a glass-fiber membrane modified with antigen, capture of a primary antibody of interest, and binding of a labeled secondary antibody to determine the primary antibody concentration using fluorescence.

this section first describes Tra19 immobilization in glass-fiber membranes modified with adsorbed polyelectrolyte layers and examines the trastuzumab-binding capacity in these modified membranes. Subsequently, using 96-well plates with mimotope-modified glass-fiber membranes, the research investigates the specific capture and detection of trastuzumab (spiked in human serum) in <5 min (including sample loading, washing, reagent binding, and fluorescence detection). Lastly, we assess the capture and quantification of a mAb against the SARS-COV-2 spike RBD protein. These analyses employ a polyhistidine-tagged SARS-CoV-2 RBD protein immobilized in the membranes of 96-well plates.

Immobilization of Tra19 in Glass-Fiber Membranes. The first step in creating porous membranes to capture specific mAbs is immobilization of a selective affinity molecule in the pores. Mimotope peptides are attractive for binding mAbs because they are relatively small molecules, easy to immobilize, and highly specific.[53−55] In prior work, we immobilized 25 ± 4 mg of the mimotope Tra19 per mL of a spongy nylon membrane.[42] The immobilization method includes adsorption of a PAA-containing film, activation of the −COOH groups of PAA, and reaction of primary amines on the mimotope, Tra19, with active esters. Continuous recirculation of solutions through 96-well plates is not feasible, so we add solutions to the wells and allow them to incubate for 5−10 min prior to vacuum filtration. Reapplication of solutions to the wells multiple times mimics the continuous flow used previously.

To quantify Tra19 immobilization, we employed 2 cm-diameter glass-fiber membranes in a home-built holder using either continuous circulation of solutions or multiple incubations and filtrations with reuse of the effluent. The latter procedure is similar to that for modifying membranes in 96-well plates, but use of the 2 cm membranes and a peristaltic pump allows more quantitative collection of effluent solutions. Analysis of the Tra19 loading solution before and after multiple incubations and passes through the membrane suggests immobilization of 2.9 ± 0.5 mg of Tra19 per mL of membrane. For comparison, the Tra19-binding capacity is 5.1 ± 1.3 mg per mL when circulating solutions through the membrane. Thus, the incubation method results in approximately 40% less Tra19 immobilization. Regardless of the mimotope immobilization procedure, the mimotope concentration in glass-fiber membranes is nearly an order of magnitude less than that observed with nylon membranes[42] presumably because of a lower surface area-to-volume ratio. Figure S1 in the Supporting Information presents SEM images of unmodified nylon and glass-fiber membranes (from wells), showing notable differences in porosity between the two substrates. The SEM images in Figures S1B and 2A show that glass-fiber membranes have a wide distribution of pores sizes with strands of different thicknesses.

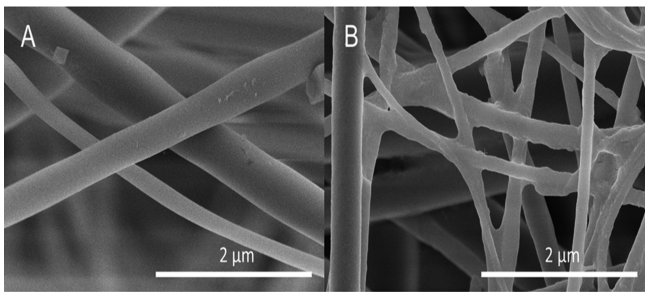

Figure 2. SEM images of (A) unmodified glass-fiber membrane and (B) $(PEI/PAA)_2$-Tra19-modified glass-fiber membrane exposed sequentially to 4 μg/mL trastuzumab in 1% human serum and fluorescently labeled secondary antibody, with rinsing between capture of each antibody. Membranes were removed from the well plate prior to sputter-coating with 5 nm of gold/palladium and imaging using a Thermo Fisher Helios G4 Ux instrument.

Comparison of high-magnification SEM images of unmodified (Figure 2A) and Tra19-modified glass-fiber membranes (after antibody capture, Figure 2B) suggests an increase in surface roughness of the glass fibers after modification and antibody capture. Figure S2 of the Supporting Information shows other SEM images of unmodified and various modified glass-fiber membranes. Previous studies showed that the thickness of $(PEI/PAA)_2$ and related films (deposited under conditions similar to this study) on flat substrates is < 30 nm.[56−58] Modification with Tra19 and capture of antibodies might double the film thickness, but the total thickness of the adsorbed material on a fiber should be at most 60 nm. However, in Figures 2B and S2, there are areas where films appear thicker than expected. Immobilization of around 3 mg of Tra19 per mL of membrane suggests that the mimotope should occupy only 0.3% of the membrane volume and have a minimal effect on membrane porosity, which is consistent with the images.

Quantifying Trastuzumab Capture in Tra19-Modified Glass-Fiber Membranes. Subsequently, we assessed the binding of trastuzumab to 2 cm membranes containing the Tra19 mimotope. Figure 3 shows trastuzumab breakthrough curves during the passage of 50 μg/mL or 100 μg/mL trastuzumab solutions through different Tra19-modified glass-fiber membranes at two flow rates. For passage of the 100 μg/mL solutions, the similar shapes of the curves obtained at 0.5 and 5 mL/min flow rates imply that capture is rapid compared to the residence time in the membrane. The shape of the curves may stem from the distribution of pore sizes in the membrane, where larger pores saturate first due to high flow rates and low surface area-to-volume ratios.

Using breakthrough curves, we determined the binding capacity by summing the products of aliquot volumes and the differences between the feed and permeate concentrations in each aliquot. The Supporting Information (Figure S3) shows replicate breakthrough curves with other membranes prepared using incubation or circulation. Breakthrough curves obtained with the 100 μg/mL trastuzumab solution indicate a capture of 1.3 ± 0.3 mg of trastuzumab per mL of membrane; the breakthrough curves with a 50 μg/mL solution show similar capacities. This is about eight-fold less trastuzumab-binding per volume than in nylon membranes that have a higher

https://doi.org/10.1021/acs.analchem.1c03654
Anal. Chem. 2022, 94, 884−891

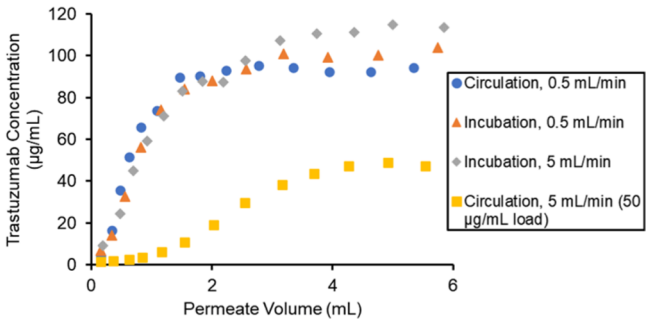

Figure 3. Concentrations of trastuzumab in the permeate passing through glass-fiber membranes modified using either circulation or serial incubations of polyelectrolyte, EDC/NHS, and Tra19 solutions. 50 μg/mL or 100 μg/mL trastuzumab feed solutions were passed through the membrane at 0.5 or 5 mL/min. Blue circles—modification using circulation of solutions and flow of a 100 μg/mL trastuzumab solution through the membrane at 0.5 mL/min. Orange triangles—modification with serial incubations of solutions and flow of a 100 μg/mL trastuzumab solution through the membrane at 0.5 mL/min. Gray diamonds—modification with serial incubations of solutions and flow of a 100 μg/mL trastuzumab solution through the membrane at 5 mL/min. Yellow squares—modification using circulation of solutions and flow of a 50 μg/mL trastuzumab solution through the membrane at 5 mL/min.

surface area per volume.[42] However, the thickness of the glass-fiber membrane in the 96-well plate is about five times the thickness of nylon membranes. Thus, for membranes with the same radius, the glass-fiber membranes in the 96-well plates should bind only 40% less trastuzumab.

Notably, membranes modified with Tra19 using circulation of solutions show the same binding capacity as membranes modified by repeatedly incubating the membrane in solutions. The slightly lower amount of Tra19 immobilization with incubation does not significantly affect trastuzumab binding. The molar ratio of bound trastuzumab to immobilized Tra19 is around 1:1500, so an increase in Tra19 density may simply result in additional mimotopes that are sterically inaccessible to antibodies.

The breakthrough curve at the lower feed concentration in Figure 3 (50 μg/mL, yellow squares) shows capture of 80% of the trastuzumab in the first 2 mL of solution passed through the membrane and ~100% capture during passage of the first mL. The volume of the 2 cm-diameter membrane in these studies is about 2.5 times that of the membrane in the 96-well plates. Thus, we estimate that the membranes in the well plates should capture >80% of the mAb in the first 0.7 mL passed through the membrane, and experiments employed a passage of 0.5 mL through a well. The capture percentage should increase further with lower concentrations if the affinity is high. Accordingly, we expect nearly quantitative capture of antibodies during a passage of 0.5 mL of solution through a membrane in a well when antibody concentrations are <30 μg/mL. Below, we limit analyses to <30 μg/mL, and more concentrated solutions will give signals outside the calibration range.

Modified 96-Well Plates for Rapid Capture and Quantitation of Trastuzumab in Serum. We next investigated the capture of trastuzumab and a fluorescently labeled secondary antibody using Tra19-modified glass-fiber membranes in 96-well plates. Measurement of the captured secondary-antibody fluorescence as a function of trastuzumab concentration in the loading solution yields a calibration curve for the determination of trastuzumab concentrations in human serum. In these experiments, we pass 0.5 mL of trastuzumab-spiked serum (undiluted or diluted 1:100) through Tra19-modified 96-well filter plates, wash with buffer, pass anti-human IgG conjugated to Cy5 through the plates, and perform a final wash before fluorescence measurement (Figure 1). With a flow rate of ~5 mL/min obtained using a vacuum manifold, this entire procedure (including loading) requires only 3 min. Quantitation then occurs in <1 additional min using a microplate reader to detect the fluorescence from the captured secondary antibody. Figure 4 shows the resulting calibration

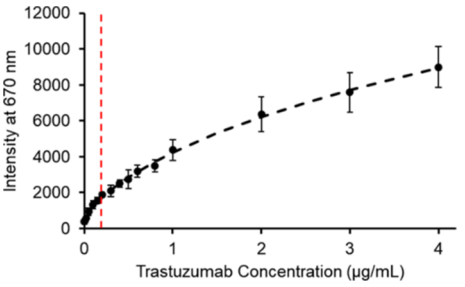

Figure 4. Calibration curve for analysis of trastuzumab spiked in 1% human serum. Analysis included capture of trastuzumab in a Tra19-modified 96-well plate, rinsing, binding of a fluorescently labeled secondary antibody, rinsing, and determination of the well fluorescence. The *y*-axis shows the fluorescence intensity of Cy5 (conjugated to the secondary antibody) at 670 nm. Error bars represent standard deviations from analyses with at least three replicate membranes. The dashed black curve is a four-parameter logistic fit to the data. The red vertical line shows the lower limit needed to ensure effective therapies. Data show results from 60 different wells with analyses occurring on three different days.

curve for trastuzumab (0.01−4 μg/mL) spiked in 1% human serum. This concentration range approximately corresponds to the concentrations found in patients (0.2−4.4 μg/mL after a 1:100 dilution).[30] As expected, the fluorescence intensity increases with the concentration of trastuzumab spiked in the loading samples. The shape of the curve indicates that the secondary-antibody binding or fluorescence does not increase proportionally to the primary antibody concentration.[59,60] The fluorescence intensity increases when passing additional secondary antibody through the membrane, so we think that the nonlinear increase in the signal appears because binding of trastuzumab begins to saturate at high concentrations.

Although the relationship between fluorescence intensity from the well and the concentration of trastuzumab in the loading solution is nonlinear, a four-parameter logistic fit allows the determination of trastuzumab concentration in serum. Note that the data show results from 60 different membranes (i.e., 60 wells) modified and examined on three different days, with no day-to-day correction. Thus, the data include well-to-well variability. For lot-to-lot variability in the plates, one would likely develop separate calibration curves for each lot. The coefficient of variation for the different points is at most 23%. The detection limit, where the signal is approximately three times the standard deviation of the blank plus the blank signal, is 0.05 μg/mL.

We then used the calibration curve to determine trastuzumab concentrations in separately prepared spiked samples. As Figure S4 in the Supporting Information shows, the differences between the average determined concentrations

https://doi.org/10.1021/acs.analchem.1c03654
Anal. Chem. 2022, 94, 884−891

(from 7 to 9 measurements) and the true concentrations are <10%, even with the calibration curve and sample measurements taken on different days. Errors are larger in single replicates. This small error should be sufficient to determine if patient concentrations are above the 20 μg/mL value (0.2 μg/mL after dilution) needed for effective treatments.[31,32,34] Effective analysis occurs even with data obtained on different days. Thus, weekly calibration may be sufficient. Given the uncertainties in analyses at high concentrations, the assay might best serve in demonstrating that trastuzumab is above a threshold level.

The concentration of trastuzumab in undiluted serum (20−440 μg/mL) is outside of the calibration range in Figure 4 (0−4 μg/mL). Nevertheless, we are interested in examining whether mAb analysis is possible in the challenging matrix of undiluted serum. Thus, we loaded 0.5 mL of human serum containing 2−30 μg/mL of trastuzumab in wells containing Tra19-modified glass-fiber membranes and subsequently captured the Cy5-labeled secondary antibody. The resulting calibration curve in Figure 5 shows a clear response to

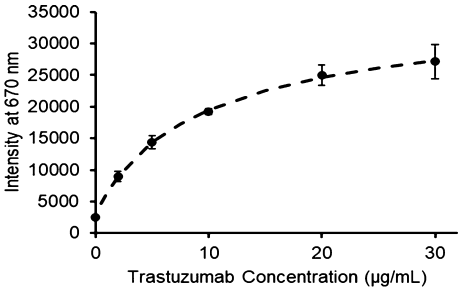

Figure 5. Calibration curve for analysis of trastuzumab spiked in undiluted pooled human serum. Analysis included capture of trastuzumab in a Tra19-modified 96-well plate, rinsing, binding of a fluorescently labeled secondary antibody, rinsing, and determination of the well fluorescence. Error bars show the standard deviations from three replicate experiments. The dashed curve is a four-parameter logistic fit to the data. Data were obtained with 18 different wells, three different wells for each concentration, and analyses on multiple days.

trastuzumab in the undiluted serum and should allow the determination of whether the trastuzumab level in a patient is above 10 μg/mL. However, the background signal (0 μg/mL trastuzumab) is 10-fold greater in undiluted serum than in 1% serum, so detection limits are much higher in undiluted serum. Unfortunately, at higher concentrations, the trastuzumab-binding sites likely become saturated, so analysis of physiological concentrations is not possible without dilution.

We also examined the capture of trastuzumab from sera of individual patients instead of from the pooled serum purchased from Sigma-Aldrich. The individual sera came from 2 male and 2 female unidentified patients. Figure S5 shows that the Cy5 intensity at 670 nm again increases with the amount of trastuzumab added. Comparing the trastuzumab calibration curve obtained with pooled serum and individual patient sera, the signal due to nonspecific binding from serum alone (y-intercept in the calibration curves) increases ∼two-fold in the individual patient sera. For data points obtained with various trastuzumab concentrations, we observe a ∼1.5-fold increase in fluorescence intensity in individual patient sera samples compared to the pooled serum samples. The higher background binding from the individual patient sera could stem from different heat and filter treatments of the pooled serum versus the patient serum. Nevertheless, the calibration curve using data from all four individual patient sera shows a coefficient of variation <8% at all spiked trastuzumab concentrations.

Selective Capture and Quantitation of an Antispike mAb from Serum. We also explored the selective capture and quantitation of a mAb to the spike RBD protein of the SARS-CoV-2 virus. These analyses include immobilization of RBD protein in the 96-well glass-fiber plate and capture of a mAb (raised against the spike RBD protein). Initially, we attached the RBD protein to PAA-modified glass-fiber membranes via reaction of activated PAA with the primary amine groups in solvent-exposed lysine residues in the RBD protein. This method immobilizes the RBD protein in random orientations, likely making some of the binding sites of the RBD protein inaccessible to the antibody. To maximize the accessibility of RBD protein to the antispike mAb, we also immobilized this protein in a more oriented fashion using a polyhistidine tag at the RBD C-terminus. In this case, we first modify the membrane with NTA-nickel complexes[51] to capture the RBD-his.

For analysis of the antispike mAb concentration, we captured it in membranes containing RBD protein and subsequently bound the Cy5-labeled secondary antibody to generate a signal. Figure 6 shows the calibration curve for this

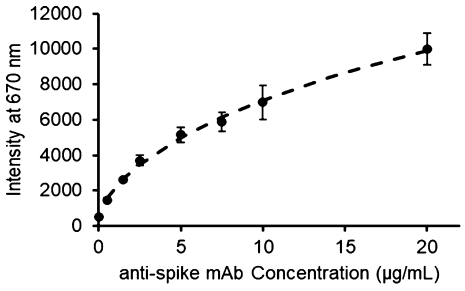

Figure 6. Calibration curve for the analysis of an antispike mAb added to 5% pooled patient sera. Assays comprise binding of antispike mAbs to an RBD-his-modified membrane in a 96-well plate, rinsing, binding of Cy5-labeled secondary antibody, rinsing, and measurement of fluorescence at 670 nm. Error bars represent the standard deviation from three replicate experiments. The dashed curve shows a four-parameter logistic fit to the data. Data were obtained with 24 different wells, three different wells for each concentration, and analyses on multiple days.

analysis, which employed 96-well plates with immobilized RBD-his in glass-fiber membranes. For comparison, Figure S6 shows the related calibration curve obtained with covalently immobilized RBD. The use of both types of immobilized RBD leads to fluorescence that increases with antispike mAb concentration, but the signal is three times higher when using the RBD-his. The detection limit is approximately 0.1 μg/mL (or 2 μg/mL before dilution). Typical analyses of "unknown" spiked samples show errors <10% for average concentrations (Figure S7), but errors are often larger in single-replicate measurements. Importantly, loading of the serum, rinsing, loading of the Cy5-labeled antibody, rinsing, and determination of fluorescence again require <5 min.

These analyses show the potential for monitoring mAb-based COVID-19 therapy. Polyclonal donor antibodies will likely be more difficult to detect due to a range of affinities.

https://doi.org/10.1021/acs.analchem.1c03654
Anal. Chem. 2022, 94, 884−891

Future work should examine detection of polyclonal antibodies to see if the technology could be useful for monitoring immunity. Such studies would need to determine the range of affinities over which the assay is effective as well as the dependence of signals on antibody affinity.

CONCLUSIONS

In this study, we successfully applied previous nylon-membrane-modification methods to glass-fiber membranes in 96-well filter plates. Binding of Cy5-labeled secondary antibodies to captured mAbs in glass-fiber membranes allows the determination of the primary mAb concentrations based on the fluorescence of Cy5. Using Tra19-modified 96-well plates, these assays have a trastuzumab analysis range that covers the clinical trough concentrations found in diluted patient serum.[30] Such assays can occur in both diluted and undiluted serum, although therapeutic trastuzumab concentrations in undiluted serum are outside the range of the technique. 96-well plates with immobilized RBD (part of the SARS-CoV-2 spike protein) allow determination of the concentration of an antispike mAb in diluted serum. Future studies with polyclonal spike protein antibodies are needed to examine the robustness of this method. Assays for both trastuzumab and the antispike mAb give average determined concentrations with an error <10%, which is sufficient for many clinical purposes.[20,61]

ASSOCIATED CONTENT

Supporting Information

The Supporting Information is available free of charge at https://pubs.acs.org/doi/10.1021/acs.analchem.1c03654.

Additional SEM images of membranes, additional breakthrough and calibration curves, plots of error in analyses, experimental procedures, and discussion of costs (PDF)

AUTHOR INFORMATION

Corresponding Author

Merlin L. Bruening − *Department of Chemistry and Biochemistry, University of Notre Dame, Notre Dame, Indiana 46556, United States; Department of Chemical and Biomolecular Engineering, University of Notre Dame, Notre Dame, Indiana 46556, United States;* orcid.org/0000-0002-4553-5143; Phone: +1 574-631-3024; Email: mbruenin@nd.edu

Authors

Hui Yin Tan − *Department of Chemistry and Biochemistry, University of Notre Dame, Notre Dame, Indiana 46556, United States*

Junyan Yang − *Department of Chemical and Biomolecular Engineering, University of Notre Dame, Notre Dame, Indiana 46556, United States*

Jacqueline C. Linnes − *Weldon School of Bioengineering, Purdue University, West Lafayette, Indiana 47907, United States;* orcid.org/0000-0003-4962-0908

Christopher J. Welch − *Indiana Consortium for Analytical Science & Engineering (ICASE), Indianapolis, Indiana 46202, United States*

Complete contact information is available at: https://pubs.acs.org/10.1021/acs.analchem.1c03654

Author Contributions

The manuscript was written through contributions of all authors. All authors have given approval to the final version of the manuscript.

Notes

The authors declare no competing financial interest.

ACKNOWLEDGMENTS

The authors are grateful to the National Science Foundation (RAPID2031090) and the NSF IUCRC Center for Bioanalytical Metrology (1916601) for funding of this work. We thank Tatyana Orlova and Dr. Karl Cronberger from the University of Notre Dame for obtaining SEM images of our membranes. We are grateful to Brandy Verhalen (Corteva) and Ivan Budyak (Eli Lilly) for helpful suggestions and editing of this manuscript.

REFERENCES

(1) Joung, H.-A.; Ballard, Z. S.; Ma, A.; Tseng, D. K.; Teshome, H.; Burakowski, S.; Garner, O. B.; Di Carlo, D.; Ozcan, A. *Lab Chip* **2019**, *19*, 1027−1034.

(2) Clarke, O. J. R.; Goodall, B. L.; Hui, H. P.; Vats, N.; Brosseau, C. L. *Anal. Chem.* **2017**, *89*, 1405−1410.

(3) Ramachandran, S.; Singhal, M.; McKenzie, K.; Osborn, J.; Arjyal, A.; Dongol, S.; Baker, S.; Basnyat, B.; Farrar, J.; Dolecek, C.; Domingo, G.; Yager, P.; Lutz, B. *Diagnostics* **2013**, *3*, 244−260.

(4) Samsonova, J. V.; Safronova, V. A.; Osipov, A. P. *Anal. Biochem.* **2018**, *545*, 43−48.

(5) Broto, M.; McCabe, R.; Galve, R.; Marco, M.-P. *Analyst* **2017**, *142*, 2404−2410.

(6) Afonso, J.; de Sousa, H. T.; Rosa, I.; Carvalho, J.; Dias, C. C.; Magro, F. *Ther. Adv. Gastroenterol.* **2017**, *10*, 661−671.

(7) Findlay, J. W. A.; Smith, W. C.; Lee, J. W.; Nordblom, G. D.; Das, I.; DeSilva, B. S.; Khan, M. N.; Bowsher, R. R. *J. Pharm. Biomed. Anal.* **2000**, *21*, 1249−1273.

(8) Kitidee, K.; Nangola, S.; Hadpech, S.; Laopajon, W.; Kasinrerk, W.; Tayapiwatana, C. *J. Virol. Methods* **2012**, *186*, 21−29.

(9) Immunoassay Market Size & Share Report, 2021−2028 http://www.grandviewresearch.com/industry-analysis/immunoassay-market (accessed Dec 10, 2021).

(10) Chen, Y.; Wu, D.; Sun, L. *Med. Sci. Monit.* **2020**, *26*, No. e919530.

(11) Yi, X.; Chen, F.; Liu, F.; Peng, Q.; Li, Y.; Li, S.; Du, J.; Gao, Y.; Wang, Y. *Stem Cell Res. Ther.* **2020**, *11*, 183.

(12) Oh, S.-H.; Choi, Y.-B.; Kim, J.-H.; Weihl, C. C.; Ju, J.-S. *Anal. Biochem.* **2017**, *530*, 57−67.

(13) Campbell, J.; Pollock, N. R.; Sharon, A.; Sauer-Budge, A. F. *Anal. Methods* **2015**, *7*, 8472−8477.

(14) Lin, C.-T.; Kuo, S.-H.; Lin, P.-H.; Chiang, P.-H.; Lin, W.-H.; Chang, C.-H.; Tsou, P.-H.; Li, B.-R. *Sens. Actuators B Chem.* **2020**, *316*, 128003.

(15) Calmo, R.; Chiadò, A.; Fiorilli, S.; Ricciardi, C. *ACS Appl. Bio Mater.* **2020**, *3*, 5787−5795.

(16) He, Z.; Huffman, J.; Curtin, K.; Garner, K. L.; Bowdridge, E. C.; Li, X.; Nurkiewicz, T. R.; Li, P. *Anal. Chem.* **2021**, *93*, 1489−1497.

(17) Kim, S. H.; Iwai, S.; Araki, S.; Sakakihara, S.; Iino, R.; Noji, H. *Lab Chip* **2012**, *12*, 4986−4991.

(18) Zschätzsch, M.; Ritter, P.; Henseleit, A.; Wiehler, K.; Malik, S.; Bley, T.; Walther, T.; Boschke, E. *Eng. Life Sci.* **2019**, *19*, 681−690.

(19) Szmacinski, H.; Smith, D. S.; Hanson, M. A.; Kostov, Y.; Lakowicz, J. R.; Rao, G. *Biotechnol. Bioeng.* **2008**, *100*, 448−457.

(20) Nugue, G.; Bidart, M.; Arlotto, M.; Mousseau, M.; Berger, F.; Pelletier, L. *PLoS One* **2013**, *8*, No. e72021.

(21) Damen, C. W. N.; de Groot, E. R.; Heij, M.; Boss, D. S.; Schellens, J. H. M.; Rosing, H.; Beijnen, J. H.; Aarden, L. A. *Anal. Biochem.* **2009**, *391*, 114−120.

(22) Imamura, C. K. *Drug Metab. Pharmacokinet.* **2019**, *34*, 14−18.

(23) Baselga, J.; Carbonell, X.; Castañeda-Soto, N.-J.; Clemens, M.; Green, M.; Harvey, V.; Morales, S.; Barton, C.; Ghahramani, P. *J. Clin. Oncol.* **2005**, *23*, 2162−2171.
(24) Cobleigh, M. A.; Vogel, C. L.; Tripathy, D.; Robert, N. J.; Scholl, S.; Fehrenbacher, L.; Wolter, J. M.; Paton, V.; Shak, S.; Lieberman, G.; Slamon, D. J. *J. Clin. Oncol.* **1999**, *17*, 2639.
(25) Berinstein, N. L.; Grillo-López, A. J.; White, C. A.; Bence-Bruckler, I.; Maloney, D.; Czuczman, M.; Green, D.; Rosenberg, J.; McLaughlin, P.; Shen, D. *Ann. Oncol.* **1998**, *9*, 995−1001.
(26) Widmer, N.; Bardin, C.; Chatelut, E.; Paci, A.; Beijnen, J.; Levêque, D.; Veal, G.; Astier, A. *Eur. J. Cancer* **2014**, *50*, 2020−2036.
(27) Vu, T.; Claret, F. X. *Front. Oncol.* **2012**, *2*, 62.
(28) Davidson, M.; Starling, N. *OncoTargets Ther.* **2016**, *9*, 7235−7245.
(29) Gunturu, K. S.; Woo, Y.; Beaubier, N.; Remotti, H. E.; Saif, M. W. *Ther. Adv. Med. Oncol.* **2013**, *5*, 143−151.
(30) Jamieson, D.; Cresti, N.; Verrill, M. W.; Boddy, A. V. *J. Immunol. Methods* **2009**, *345*, 106−111.
(31) De Santes, K.; Slamon, D.; Anderson, S. K.; Shepard, M.; Fendly, B.; Maneval, D.; Press, O. *Cancer Res.* **1992**, *52*, 1916−1923.
(32) Pegram, M.; Hsu, S.; Lewis, G.; Pietras, R.; Beryt, M.; Sliwkowski, M.; Coombs, D.; Baly, D.; Kabbinavar, F.; Slamon, D. *Oncogene* **1999**, *18*, 2241−2251.
(33) Bruno, R.; Washington, C. B.; Lu, J.-F.; Lieberman, G.; Banken, L.; Klein, P. *Cancer Chemother. Pharmacol.* **2005**, *56*, 361−369.
(34) Cosson, V. F.; Ng, V. W.; Lehle, M.; Lum, B.L. *Cancer Chemother. Pharmacol.* **2014**, *73*, 737−747.
(35) Yang, J.; Zhao, H.; Garnett, C.; Rahman, A.; Gobburu, J. V.; Pierce, W.; Schechter, G.; Summers, J.; Keegan, P.; Booth, B.; Wang, Y. *J. Clin. Pharmacol.* **2013**, *53*, 160−166.
(36) Beigel, J. H.; et al. *N. Engl. J. Med.* **2020**, *383*, 1813−1826.
(37) Goldman, J. D.; et al. *N. Engl. J. Med.* **2020**, *383*, 1827−1837.
(38) Spinner, C. D.; et al. *JAMA* **2020**, *324*, 1048−1057.
(39) Gottlieb, R. L.; et al. *JAMA* **2021**, *325*, 632−644.
(40) Joyner, M. J.; et al. *Mayo Clin. Proc.* **2020**, *95*, 1888−1897.
(41) Joyner, M. J.; et al. Effect of Convalescent Plasma on Mortality among Hospitalized Patients with COVID-19: Initial Three-Month Experience. **2020**, medRxiv:2020.08.12.20169359.
(42) Liu, W.; Bennett, A. L.; Ning, W.; Tan, H.-Y.; Berwanger, J. D.; Zeng, X.; Bruening, M. L. *Anal. Chem.* **2018**, *90*, 12161−12167.
(43) Berwanger, J. D.; Tan, H. Y.; Jokhadze, G.; Bruening, M. L. *Anal. Chem.* **2021**, *93*, 7562−7570.
(44) Schwark, S.; Sun, W.; Stute, J.; Lütkemeyer, D.; Ulbricht, M.; Sellergren, B. *RSC Adv.* **2016**, *6*, 53162−53169.
(45) Chenette, H. C. S.; Welsh, J. M.; Husson, S. M. *Sep. Sci. Technol.* **2017**, *52*, 276−286.
(46) Wang, J.; Zhou, J.; Gowtham, Y. K.; Harcum, S. W.; Husson, S. M. *Biotechnol. Prog.* **2017**, *33*, 658−665.
(47) Suresh, P.; Duval, C. E. *Ind. Eng. Chem. Res.* **2020**, *59*, 12212−12222.
(48) Bhattacharjee, S.; Dong, J.; Ma, Y.; Hovde, S.; Geiger, J. H.; Baker, G. L.; Bruening, M. L. *Langmuir* **2012**, *28*, 6885−6892.
(49) Bruening, M. L., Wijeratne, S., Ning, W., Dong, J., Liu, W. Polyacid-Functionalized Porous Membranes, Related Methods, and Related Polyacid Polymers. U.S. Patent 073,565 A1, 2016.
(50) Shang, Y.; Singh, P. R.; Chisti, M. M.; Mernaugh, R.; Zeng, X. *Anal. Chem.* **2011**, *83*, 8928−8936.
(51) Wijeratne, S.; Liu, W.; Dong, J.; Ning, W.; Ratnayake, N. D.; Walker, K. D.; Bruening, M. L. *ACS Appl. Mater. Interfaces* **2016**, *8*, 10164−10173.
(52) GeminiBio. Heat Inactivation of Serum. http://www.gembio.com/post/heat-inactivation-serum (accessed Dec 10, 2021).
(53) Peltomaa, R.; Agudo-Maestro, I.; Más, V.; Barderas, R.; Benito-Peña, E.; Moreno-Bondi, M. C. *Anal. Bioanal. Chem.* **2019**, *411*, 6801−6811.
(54) Chen, X.; Ding, X.; Zhu, L.; Zhang, G. *Int. J. Biol. Macromol.* **2021**, *183*, 2376−2386.
(55) Shi, W.; Zhao, L.; Xu, Y.; Xu, G.; Zeng, Y. *Biotechnol. Biotechnol. Equip.* **2019**, *33*, 1034−1041.
(56) Shiratori, S. S.; Rubner, M. F. *Macromolecules* **2000**, *33*, 4213−4219.
(57) Yang, Y.-H.; Haile, M.; Park, Y. T.; Malek, F. A.; Grunlan, J. C. *Macromolecules* **2011**, *44*, 1450−1459.
(58) Ma, Y.; Dong, J.; Bhattacharjee, S.; Wijeratne, S.; Bruening, M. L.; Baker, G. L. *Langmuir* **2013**, *29*, 2946−2954.
(59) Gao, Z.-Y.; Zhang, Q.-L.; Shi, C.; Gou, J.-X.; Gao, D.; Wang, H.-B.; Yao, S.-J.; Lin, D.-Q. *Sep. Purif. Technol.* **2020**, *253*, 117554.
(60) Feidl; Garbellini; Luna; Vogg; Souquet; Broly; Morbidelli; Butté. *Processes* **2019**, *7*, 683.
(61) McBride, J. M.; Lim, J. J.; Burgess, T.; Deng, R.; Derby, M. A.; Maia, M.; Horn, P.; Siddiqui, O.; Sheinson, D.; Chen-Harris, H.; Newton, E. M.; Fillos, D.; Nazzal, D.; Rosenberger, C. M.; Ohlson, M. B.; Lambkin-Williams, R.; Fathi, H.; Harris, J. M.; Tavel, J. A. *Antimicrob. Agents Chemother.* **2017**, *61*, No. e01154.

https://doi.org/10.1021/acs.analchem.1c03654
Anal. Chem. 2022, 94, 884−891